

# From Instantons to Sphalerons: Time-dependent Periodic Solutions of SU(2)-Higgs Theory

Keith L. Frost and Laurence G. Yaffe

*University of Washington, Department of Physics, Seattle, Washington 98105-1560*

(October 19, 2018)

## Abstract

We solve numerically for periodic, spherically symmetric, classical solutions of SU(2)-Higgs theory in four-dimensional Euclidean space. In the limit of short periods the solutions approach tiny instanton–anti-instanton superpositions while, for longer periods, the solutions merge with the static sphaleron. A previously predicted bifurcation point, where two branches of periodic solutions meet, appears for Higgs boson masses larger than  $3.091 M_W$ .

## I. INTRODUCTION

In electroweak theory, baryon number non-conserving processes are a consequence of topological transitions in which there is an order one change in the Chern-Simons number of the SU(2) gauge field. At zero temperature, such transitions are quantum tunneling events, and the rate of these transitions is directly related to the classical action of instanton solutions of SU(2) gauge theory [1]. At sufficiently high temperatures,<sup>1</sup> the dominant mechanism for baryon number violation involves classical thermally activated transitions over the potential energy barrier separating inequivalent vacuum states. The configuration characterizing the top of the barrier is the static sphaleron solution of SU(2)-Higgs theory [2]; the energy of this solution controls the thermally-activated transition rate [3,4].

When one lowers the temperature from the sphaleron dominated regime, the topological transition rate is related to the action of time-dependent periodic classical solutions of the Euclidean field equations with a period  $\beta$  equal to the inverse temperature.<sup>2</sup> For convenience, we will refer to such solutions as periodic “bounces”.<sup>3</sup>

---

<sup>1</sup>But below the cross-over (or critical) temperature where “broken” electroweak symmetry is restored.

<sup>2</sup>In SU(2)-Higgs theory, configurations resembling the zero-size limit of instantons and anti-instantons also play a role in determining the transition rate at sufficiently low temperatures [1,5,6].

<sup>3</sup>Coleman [7] used the term “bounce” to refer to a time-dependent Euclidean classical solution beginning and ending at a (metastable) local minimum of the potential. Our usage is a generalization.

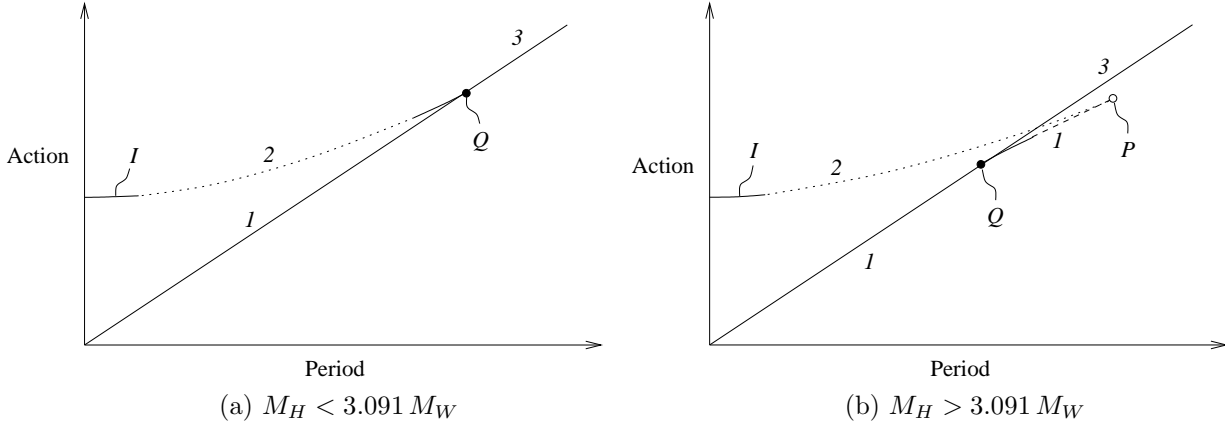


FIG. 1. The simplest consistent scenario for the behavior of periodic solutions in SU(2)-Higgs theory. The straight line through the origin represents the static sphaleron, whose action is simply its energy times the period. The line labeled  $I$  denotes the branch of instanton–anti-instanton solutions whose action, in the limit of vanishing period, approaches  $4\pi/\alpha_W$ . The number next to each curve indicates the number of unstable modes of the solution. Plot (a) illustrates the situation when the Higgs mass is less than  $3.091 M_W$ . A branch of bounce solutions emerges from the sphaleron at a critical period, and moves toward shorter period and lower action as the deviation from the sphaleron increases. As indicated by the dotted line, it is consistent to imagine that these limiting forms are the two ends of a single branch of solutions. Plot (b) illustrates the situation when the Higgs mass is larger than  $3.091 M_W$ . In this case, a branch of bounce solutions emerges from the sphaleron at the critical period, and moves toward longer period and larger action as the deviation from the sphaleron increases. The simplest consistent scenario is for a single additional bifurcation, marked  $P$ , to exist, at which the branch of bounces coming from the sphaleron merges with the branch of instanton–anti-instanton solutions.

In a previous paper, we used time-dependent classical perturbation theory to study periodic bounce solutions which are small deformations of the static sphaleron [6]. We found that for sufficiently small Higgs boson mass,  $M_H < 3.091 M_W$ , bounce solutions which are small oscillations about the sphaleron have an action (per period) larger than that of the sphaleron. In a plot of action versus period, this branch of bounce solutions lies above the static sphaleron line, and merges with the sphaleron at its critical period, as shown in Fig. 1a. For short periods,  $\beta \ll M_W^{-1}$ , one can find the asymptotic form of periodic solutions resembling an alternating array of instantons and anti-instantons, where the attractive instanton–anti-instanton interactions exactly counterbalance the tendency of each instanton and anti-instanton to shrink [8,6]. In the short-period limit, the resulting instanton size is

$$\rho(\beta) = \sqrt{2}M_W \left( \frac{\beta}{2\pi} \right)^2 [1 + \mathcal{O}(M_W\beta)], \quad (1.1)$$

and the action (per period) is

$$S(\beta) = \frac{1}{g^2} \left[ 16\pi^2 + \frac{M_W^4\beta^4}{2\pi^2} + \mathcal{O}(M_W^5\beta^5) \right]. \quad (1.2)$$

Both the bounce solutions, and these instanton–anti-instanton solutions, have two negative modes in their small fluctuation spectra [6]. For  $M_H < 3.091 M_W$ , it is reasonable to conjecture that a single branch of periodic solutions joins these two limiting forms, as illustrated in Fig. 1a.

For Higgs boson masses above  $3.091 M_W$ , the branch of bounce solutions which emerge from the sphaleron extends to longer period from the sphaleron bifurcation point, and the

action of these bounces lies below the action of the sphaleron (for the same period), as shown in Fig. 1b. These bounce solutions have a single negative mode in their small fluctuation spectra [6]. It is impossible for short-period instanton–anti-instanton solutions to smoothly join with these bounce solutions. The simplest consistent scenario, illustrated in Fig. 1b, is for there to be one additional bifurcation point (in the space of spherically symmetric, periodic solutions) at which the bounce solutions from the sphaleron merge with the instanton–anti-instanton solutions.

In this paper, we present results of a numerical calculation of periodic, spherically-symmetric, bounce solutions in SU(2)-Higgs theory. Our goal was to find, and follow, the different branches of periodic bounce solutions as both the period, and the Higgs mass, are varied, and to see how these solutions interpolate between the sphaleron and small instanton–anti-instanton superpositions. We found that the conjectured behavior illustrated in Fig. 1 is, in fact, correct. While preparing this manuscript, it came to our attention that similar work has been done by Bonini *et al.* [9]. Their results are consistent with ours.

We considered SU(2) gauge theory in 3+1 dimensions with a single Higgs scalar in the fundamental representation. This model represents the bosonic sector of the standard model of the weak interactions in the limit of small weak mixing angle. The action may be written in the form<sup>4</sup>

$$S = \frac{1}{g^2} \int d^4x \left[ -\frac{1}{2} \text{Tr}(F_{\mu\nu}F^{\mu\nu}) + (D_\mu\Phi)^\dagger D^\mu\Phi + \frac{M_H^2}{8M_W^2} (\Phi^\dagger\Phi - 2M_W^2)^2 \right]. \quad (1.3)$$

The scalar field  $\Phi$  is an SU(2) doublet with covariant derivative  $D_\mu = (\partial_\mu + A_\mu)$ , where  $A_\mu \equiv A_\mu^a \tau^a / 2i$ . The gauge field strength is the commutator  $F_{\mu\nu} = [D_\mu, D_\nu]$ . When restricted to spherically symmetric fields, the action (1.3) reduces to the two-dimensional form [10]

$$S = \frac{4\pi}{g^2} \int dr d\tau \left[ \frac{1}{4} r^2 f_{\mu\nu} f^{\mu\nu} + |D\chi|^2 + r^2 |D\phi|^2 + \frac{M_H^2}{8M_W^2} r^2 (|\phi|^2 - 2M_W^2)^2 + \frac{1}{2r^2} (|\chi|^2 - 1)^2 + \frac{1}{2} |\phi|^2 (|\chi|^2 + 1) - \text{Re}(\chi^* \phi^2) \right], \quad (1.4)$$

where  $\phi$  is a complex scalar which represents the spherically symmetric Higgs field,  $\chi$  is a complex scalar representing the spherically symmetric transverse modes of the gauge fields, and  $f_{\mu\nu}$  is a two-dimensional U(1) field strength tensor. After reduction to spherically symmetric form, the original classical SU(2) gauge theory becomes a classical U(1) gauge theory in 1+1 dimensions. The field  $\phi$  has a U(1) charge of 1/2, while  $\chi$  has U(1) charge 1. Note that finite action configurations must satisfy  $|\chi| \rightarrow 1$  as  $r \rightarrow 0$ , and  $|\phi| \rightarrow \sqrt{2}M_W$ ,  $|\chi| \rightarrow 1$  with  $\chi^* \phi^2$  real and positive as  $r \rightarrow \infty$ .

## II. NUMERICAL METHODS

To perform calculations with the two-dimensional action (1.4), we chose to fix radial gauge,  $a_1 = 0$ . We used a spatial discretization which is uniform in the transformed variable

---

<sup>4</sup>For convenience, we have rescaled the gauge and Higgs fields so that the action has an overall  $1/g^2$ . The conventional Higgs vacuum expectation value is  $v = 2M_W/g$ , and the usual quartic coupling is  $\lambda = \frac{1}{8}g^2 M_H^2/M_W^2$ . As usual, the weak fine-structure constant is  $\alpha_W \equiv g^2/4\pi$ .

$$s = \ln \left[ \frac{1 + Mr}{1 + mr} \right] / \ln(M/m), \quad (2.1)$$

with

$$\begin{aligned} m &\equiv \max \left\{ \frac{1}{2} \rho(\beta)^{-1}, \frac{1}{2} M_W \right\}, \\ M &\equiv \max \{ 2m, M_H \}. \end{aligned} \quad (2.2)$$

The transformation (2.1) maps the semi-infinite line  $0 \leq r < \infty$  onto the unit interval  $0 \leq s < 1$ , with an approximately logarithmic distribution of points in  $r$  for scales in between  $M^{-1}$  and  $m^{-1}$ . The long distance scale  $m^{-1}$  was set to the shorter of  $2M_W^{-1}$  and  $2\rho(\beta)$ , where  $\rho(\beta)$ , given in Eq. (1.1), is the leading-order size of an instanton stabilized against collapse in the instanton–anti-instanton periodic solution with period  $\beta$ . The short distance scale  $M^{-1}$  was chosen to equal the shorter of  $m^{-1}/2$  and  $M_H^{-1}$ . We found that this choice of discretization smoothly encompassed the different spatial scales which are most relevant in periodic bounce solutions as the parameters  $M_H$  and  $\beta$  are varied. After changing variables from  $r$  to  $s$ , spatial derivatives in the action (1.4) were replaced by nearest-neighbor finite differences. Calculations were performed using  $L = 64$  points for the spatial discretization, and the resulting discretization error in, for example, the sphaleron mass was less than one part in  $10^4$ .

Since we were looking for solutions with periodic time dependence, we chose to expand the time dependence of fields in a (truncated) Fourier series. For bounce solutions which are close to the static sphaleron, extremely accurate calculations can be performed using only a few Fourier components in each field.<sup>5</sup> As these solutions are followed toward very short periods, one finds that they approach instanton–anti-instanton superpositions in which the instanton (and anti-instanton) size shrinks quadratically with period as shown in Eq. (1.1). Consequently, as the period decreases, an increasing number of Fourier components are needed to accurately represent the time dependence.

For numerical purposes, it is convenient to separate the complex fields  $\chi$  and  $\phi$  into real and imaginary parts,

$$\chi \equiv \alpha + i\beta, \quad \phi \equiv \mu + i\nu. \quad (2.3)$$

Table I shows which fields change sign under the action of the discrete symmetries of time-reversal and parity [which is U(1) charge conjugation in the 1+1 dimensional theory (1.4)], and the resulting form of the truncated Fourier series. The bounce solutions are time reversal invariant, so only cosine terms are needed for the time-reversal even fields, and only sine terms for the time-reversal odd field  $a_0$ . The solutions are also invariant under the combination of parity plus time translation by half a period.<sup>6</sup> Because of this additional

---

<sup>5</sup>In classical perturbation theory about the sphaleron, the  $n$ -th harmonic of the fundamental frequency is only generated at  $n$ -th order in time-dependent perturbation theory [6].

<sup>6</sup>These symmetries imply that the solutions reach “turning-point” configurations, in which the time-reversal odd fields vanish, twice during each period. The two turning-point configurations are parity reflections of each other, and occur half a period apart.

discrete symmetry,<sup>7</sup> only even frequencies appear in the Fourier expansions of parity even fields, and only odd frequencies in the Fourier series for parity odd fields. Each Fourier series was truncated after  $N$  (non-zero) terms; practical computations ranged from  $N = 4$  to  $N = 64$  terms.

Field	P	T	Truncated Fourier Series
$\alpha(r, \tau)$	+	+	$\sum_{n=0}^{N-1} \alpha^{(2n)}(r) \cos[2n\omega\tau]$
$\mu(r, \tau)$	+	+	$\sum_{n=0}^{N-1} \mu^{(2n)}(r) \cos[2n\omega\tau]$
$\beta(r, \tau)$	-	+	$\sum_{n=0}^{N-1} \beta^{(2n+1)}(r) \cos[(2n+1)\omega\tau]$
$\nu(r, \tau)$	-	+	$\sum_{n=0}^{N-1} \nu^{(2n+1)}(r) \cos[(2n+1)\omega\tau]$
$a_0(r, \tau)$	-	-	$\sum_{n=0}^{N-1} a_0^{(2n+1)}(r) \sin[(2n+1)\omega\tau]$

TABLE I. Symmetry properties, and truncated Fourier series, of two-dimensional real field components.  $P$  is parity (or equivalently  $U(1)$  charge conjugation),  $T$  is time reversal, and a + or - indicates whether the field is even or odd, respectively, under the symmetry. The fundamental angular frequency  $\omega \equiv 2\pi/\beta$ , where  $\beta$  is the period. Only even harmonics occur in the expansions of parity even fields, and only odd harmonics appear in parity odd fields.

Once the radial dependence of the fields is replaced with an  $L$ -point discretization, and the time dependence restricted to an  $N$ -term Fourier series, the action (1.4) becomes a function of a finite number ( $5NL$ ) of variables. The gradient of the action,  $\delta S$ , is a  $5NL$ -component vector, and the curvature of the action,  $\delta^2 S$ , is a  $5NL$ -dimensional matrix with block band-diagonal structure. An iterative Newton method, based on steps for which

$$\delta(\text{fields}) = -(\delta^2 S)^{-1} \cdot \delta S, \quad (2.4)$$

was used to find stationary points of the action. The block band-diagonal structure of the curvature matrix  $\delta^2 S$  was used to minimize computation and memory requirements for the calculation.

---

<sup>7</sup>In our previous paper [6], we described the effect of discrete symmetries on the negative modes of the bounce and instanton–anti-instanton solutions incorrectly. Both negative modes of the instanton–anti-instanton and the bounce are time-reversal even. But the negative mode of the instanton–anti-instanton given by moving the instanton and anti-instanton closer together in imaginary time is odd under the combination of parity with time translation by half a period. The static negative mode of the sphaleron (and hence the quasi-static negative mode of the bounce) is also odd under parity combined with  $\beta/2$  time translation. The other negative mode of the instanton–anti-instanton, given by a symmetric alteration of the sizes of the instanton and anti-instanton, is even under parity combined with  $\beta/2$  time translation, as is the second negative mode (corresponding to changing the amplitude of oscillations about the sphaleron) of the branch of bounces with two negative modes.

For stability of the calculation, especially near bifurcations, it was important to guard against taking Newton steps that were too large. (That is, larger than the domain of validity of a local quadratic approximation to the action, upon which the Newton iteration (2.4) is based.) We adopted the strategy of scaling down the size of a step as needed to guarantee that the magnitude of the gradient of the action actually decreased upon taking each step.

For each value of the Higgs mass, to find the branch of solutions which merge with the sphaleron, we first found the sphaleron solution [2,11,12,6], and set the period  $\beta$  equal to the period of infinitesimal oscillations about the sphaleron, as calculated by time-dependent perturbation theory [6]. We then shifted the period  $\beta$  a small amount, in the direction indicated by the perturbative calculation, and added the first- and second-order perturbative terms to the sphaleron fields to construct an initial guess for the oscillating solution. Newton's iteration steps were then taken until the fields converged, and the gradient vanished, to within the limits of numerical accuracy. A small modification of the period  $\beta$  was then introduced, and Newton's method again used to solve for the classical fields at the new period. We used linear extrapolation in  $\beta$  to guess trial values of the fields after each change in period. The step size in  $\beta$  was automatically adjusted to the largest change which would allow Newton's method to converge in a reasonable number of steps using linearly extrapolated starting points.

As calculations ventured farther from the sphaleron solution, additional Fourier components were required to accurately represent the time-dependence of the fields. A useful check on the accuracy of the calculation proved to be the computation of the continuum Euclidean conserved energy as a function of time. For continuum classical fields, it is of course conserved. As the cutoff in the Fourier modes becomes a more significant source of error, small fluctuations in the energy grow. We set a threshold of  $\delta E/E \sim 10^{-4}$  in the relative fluctuations in the energy which the accuracy of our calculation allowed. When the fluctuations in the energy surpassed this, we doubled the number of Fourier components used in the calculation, up to a maximum of  $N = 64$  components.

To find branches of solutions which were not directly connected to the sphaleron, we first followed, for small Higgs mass  $M_H \sim M_W$ , the branch of solutions which is connected to the sphaleron down to periods  $\beta \sim M_W^{-1}$ , where they approach isolated instantons and anti-instantons. These solutions are relatively insensitive to the Higgs boson mass. It was then a simple matter to increase the Higgs boson mass into the range  $M_H > 3.091 M_W$ , and then follow the solutions back toward longer period (where they no longer merge directly with the sphaleron) using the same linear extrapolation and Newton iteration techniques to vary the period  $\beta$ .

### III. RESULTS

We display in Fig. 2 representative contour plots showing the action density of periodic solutions at four different periods, with the Higgs boson mass  $M_H = M_W$ . For Higgs boson masses this small, as discussed above, the more pronounced the oscillation in imaginary time is, the shorter the period becomes. Figure 2 shows the gradual progression from small, well-separated instanton-anti-instanton solutions with period  $\beta \sim 1/M_W$ , up to fairly small oscillations about the static sphaleron with period  $\beta = 4/M_W$ . For  $M_H = M_W$ , the periodic bounce solutions merge with the static sphaleron solutions at the period  $\beta_0 \approx 4.1695/M_W$ .

Figure 3 contains two plots of action versus period, which show the periodic Euclidean classical solutions of SU(2)-Higgs theory for  $M_H = M_W$  and  $M_H = 3 M_W$ , respectively. Note that the instanton–anti-instanton limit  $I$  is connected smoothly to the small oscillations  $J$  about the sphaleron  $K$ , by the solid curve of bounce solutions. This simple picture undergoes no fundamental change until  $M_H$  exceeds  $3.091 M_W$ .

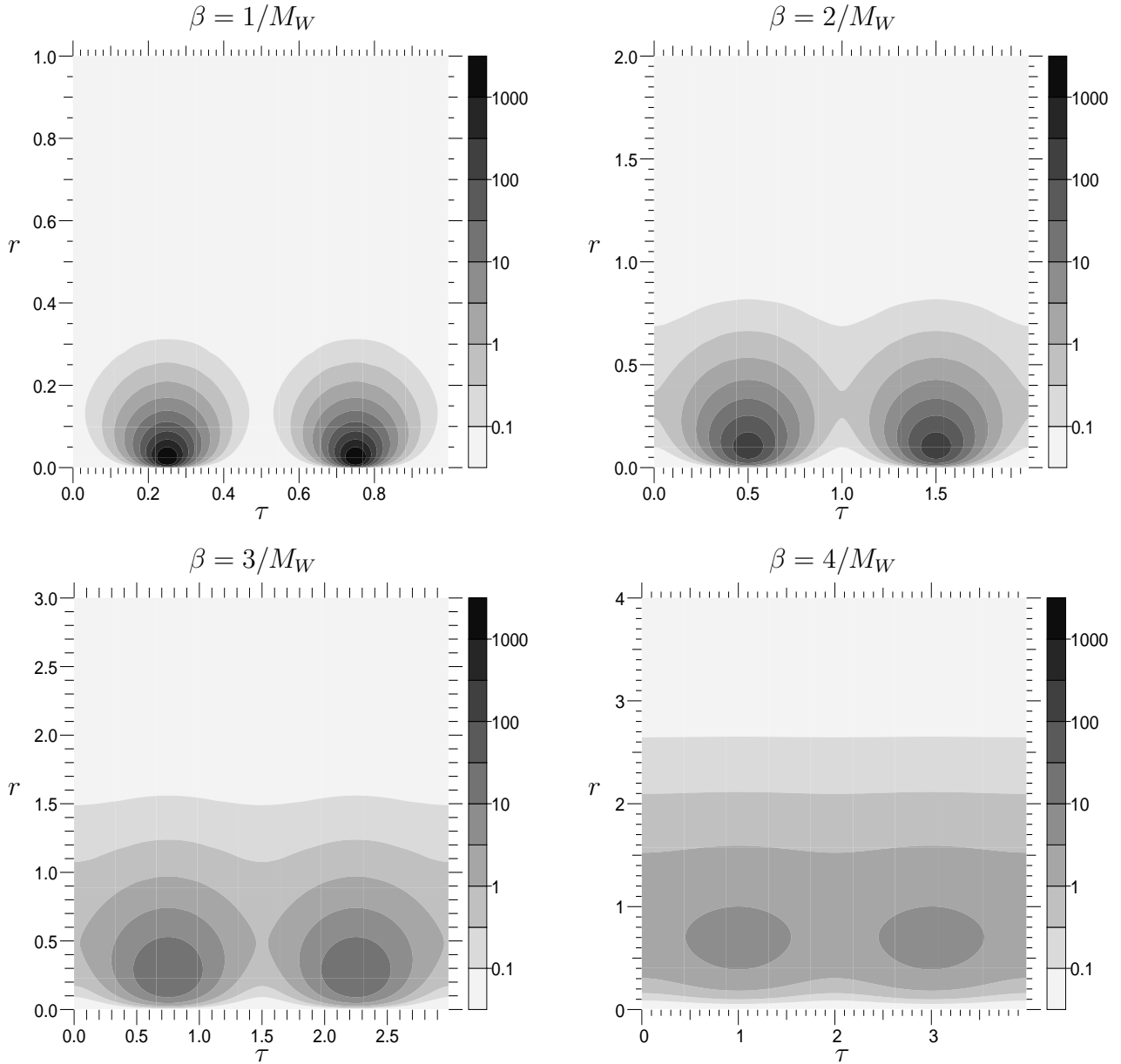


FIG. 2. Contour plots of the two-dimensional action density of bounce solutions of SU(2)-Higgs theory, as functions of radius  $r$  and imaginary time  $\tau$ . The Higgs boson mass is set to  $M_H = M_W$ , and the units are fixed to  $M_W = 1$ . The density shown is the integrand in the expression for the two-dimensional action (1.4). For Higgs boson mass  $M_H < 3.091 M_W$ , shorter periods correspond to progressively more pronounced oscillations in imaginary time, culminating in tiny, well-separated instanton–anti-instanton configurations for  $\beta \sim 1/M_W$ , as shown at the upper left. For Higgs boson mass  $M_H = M_W$ , at a period  $\beta_0 \approx 4.1695/M_W$ , the periodic solutions merge with the static sphaleron. The configuration at the lower right, with  $\beta = 4/M_W$ , consists of relatively small oscillations about the static sphaleron.

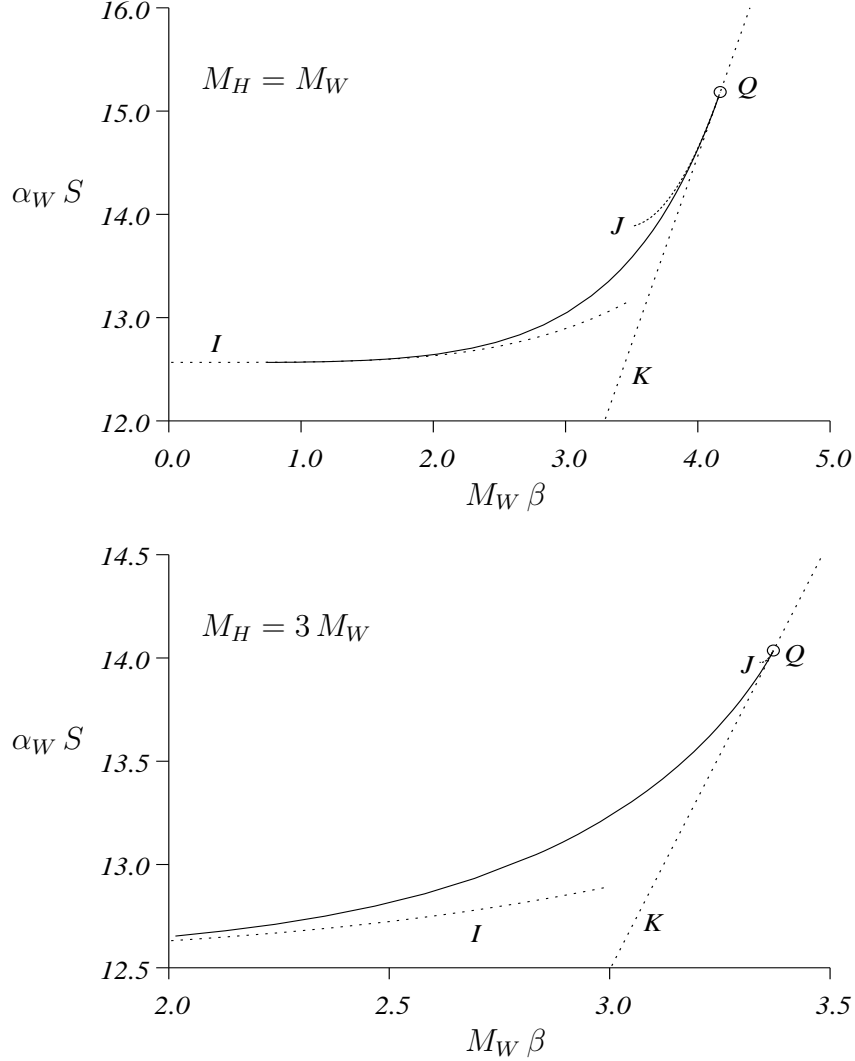


FIG. 3. The action versus the period of SU(2)-Higgs bounce solutions are plotted as solid curves. Dotted curves  $I$  show the asymptotic forms for instanton-anti-instanton solutions. Dotted curves  $J$  indicate the leading-order calculation of small oscillations about the sphaleron, while dotted line  $K$  is the sphaleron solution. The small oscillations  $J$  merge with the sphaleron  $K$  at bifurcation point  $Q$ . The upper graph shows a wide range of periods for  $M_H = M_W$ , while the lower graph provides a more detailed view near the bifurcation point  $Q$  for  $M_H = 3 M_W$ .

When the Higgs boson mass  $M_H > 3.091 M_W$ , a second bifurcation point  $P$  appears, dividing the bounce solutions into two curves on a plot of action vs. period. We calculated this bifurcation point explicitly for  $M_H = 3.2 M_W$ , and for several larger Higgs boson masses. Figure 4 shows the two branches of bounce solutions as solid curves on plots of action versus period, for  $M_H = 4 M_W$  and  $M_H = 6.665 M_W$ . For  $M_H > 6.665 M_W$ , the original bifurcation  $Q$ , which joins the bounce solutions to the sphaleron, has an action below the singular instanton-anti-instanton configuration.



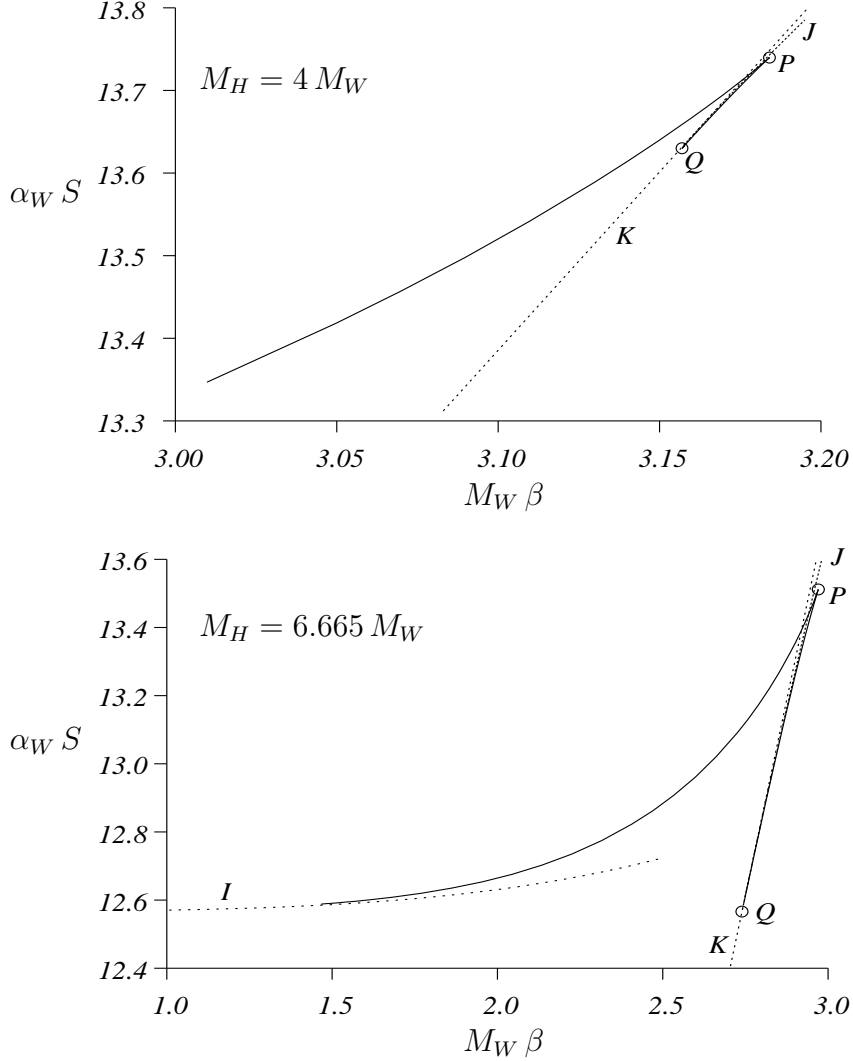


FIG. 4. Plots of action versus period of SU(2)-Higgs bounce solutions for Higgs boson masses  $M_H = 4 M_W$  and  $M_H = 6.665 M_W$ . The solid curves, meeting at bifurcation point  $P$ , are the two branches of bounce solutions. Dotted curve  $I$  shows the asymptotic form of the instanton–anti-instanton solutions. Dotted curves  $J$  indicate the leading-order calculation of small oscillations about the sphaleron, while dotted line  $K$  is the sphaleron solution. The small oscillations  $J$  merge with the sphaleron  $K$  at bifurcation point  $Q$ , whose action, at the Higgs boson mass  $M_H \approx 6.665 M_W$ , is the same as that of the zero size limit of the instanton–anti-instantons  $I$ . Bifurcation point  $P$  was predicted to exist, by the perturbative calculation shown as  $J$ , for all Higgs boson masses  $M_H > 3.091 M_W$ ; we located it explicitly for a Higgs boson mass as small as  $M_H = 3.2 M_W$ .

The period, action, and turning-point energy at the bifurcation points  $P$  and  $Q$  are plotted in Fig. 5 as functions of the Higgs boson mass  $M_H$ . The bifurcation point  $P$  was found by increasing the period  $\beta$  along each branch, using linear extrapolation followed by Newton iteration, until this method failed to converge no matter how small the step in  $\beta$ . We confirmed that the bifurcation was reached by comparing the last solution on each branch.

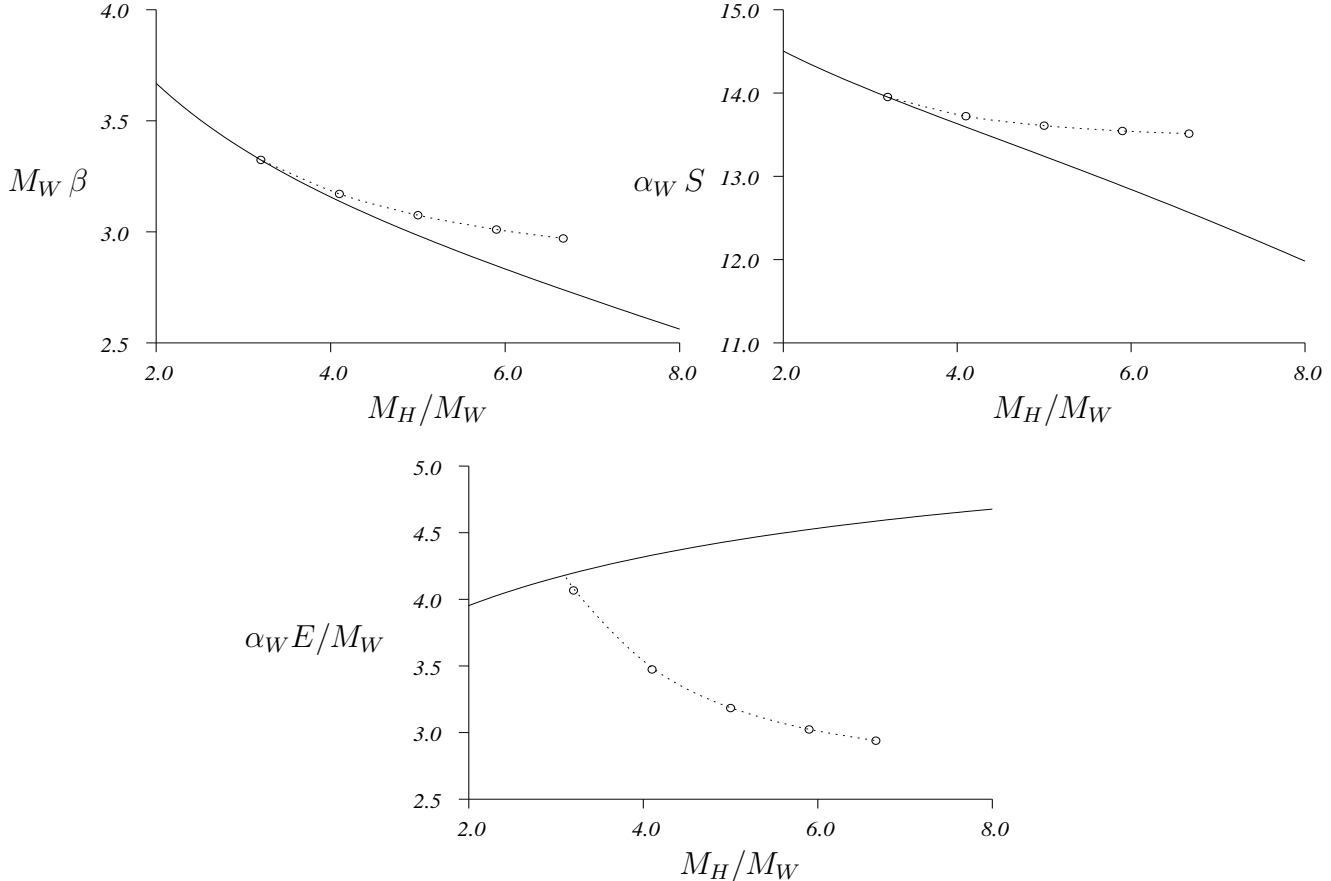


FIG. 5. The calculated period  $\beta$ , action  $S$ , and turning point energy  $E$  of the bounce bifurcation point  $P$  are plotted as circles, as functions of the Higgs boson mass  $M_H$ . The dotted lines are cubic spline fits to the calculated points. The solid lines show the corresponding values of the sphaleron bifurcation point  $Q$ .

At short periods  $\beta \lesssim 1/M_W$ , the bounce solutions approach small instanton–anti-instanton configurations. The limit to the accuracy of our computation in this region proved to be the number of Fourier components in time we could afford. With  $N = 64$  components, we could calculate with relative errors in the Euclidean energy of no more than  $\delta E/E \sim 10^{-3}$  down to periods  $\beta \approx 0.75/M_W$ . The calculated fields are compared to analytic instanton fields [see Eqn. (3.2) below] in Figs. 6 and 7.

For sufficiently short periods, one can find analytically the asymptotic form of periodic Euclidean solutions of SU(2)-Higgs theory resembling chains of alternating instantons and anti-instantons. To leading order, the fields of an instanton centered at the origin in singular gauge are [1]

$$A_\mu(x) = \frac{2\rho^2}{x^2(\rho^2 + x^2)} \bar{\eta}_{\mu\nu}^a x_\nu (\tau^a/2i) [1 + \mathcal{O}(M_W x)], \quad (3.1a)$$

$$\Phi(x) = \frac{\sqrt{2}M_W x}{\sqrt{x^2 + \rho^2}} \xi [1 + \mathcal{O}(M_W x) + \mathcal{O}(M_H x)], \quad (3.1b)$$

where  $\xi$  is an arbitrary complex unit doublet, and  $\bar{\eta}_{\mu\nu}^a$  denotes 't Hooft's  $\eta$  symbol [1]. Converting the instanton fields (3.1) into gauge-invariant two-dimensional quantities, we find

$$|\phi|^2 = \frac{2M_W^2}{1 + \rho^2/x^2}, \quad f_{01} = \frac{4\rho^2}{[\rho^2 + x^2]^2}, \quad (3.2a)$$

$$|\chi|^2 = 1 - \frac{4r^2\rho^2}{[\rho^2 + x^2]^2}, \quad \text{Re}(\chi^*\phi^2) = |\phi|^2 \left( 1 - \frac{2r^2\rho^2}{x^2[\rho^2 + x^2]} \right). \quad (3.2b)$$

The agreement between the numerical results for  $M_H = M_W$  and  $\beta = 0.75/M_W$  and the asymptotic form (3.2) shown in Figs. 6 and 7 convincingly demonstrates that the numerical solutions have reached the instanton–anti-instanton domain.

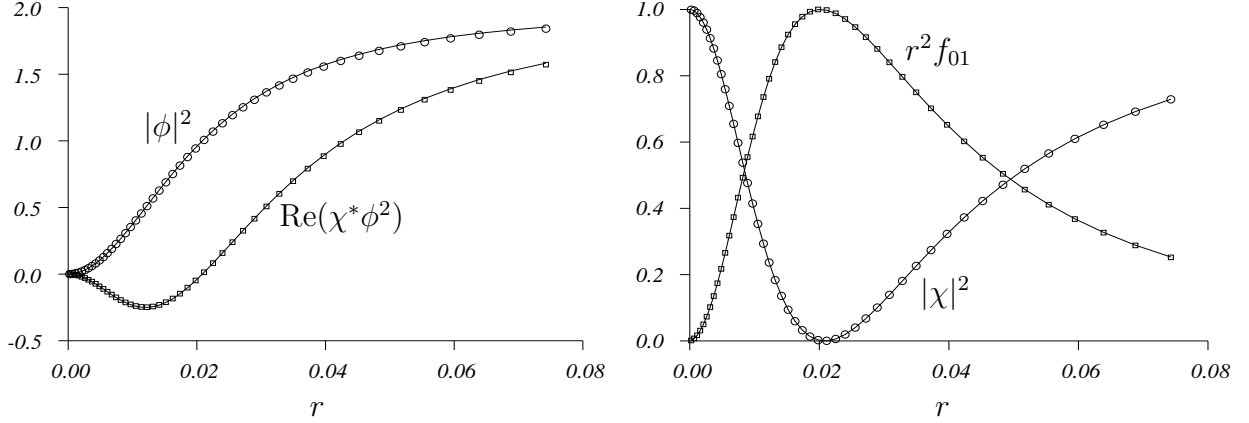


FIG. 6. The numerical bounce solutions approach instanton–anti-instanton fields, for small period ( $\beta = 0.75/M_W$ ). The circles and squares show numerically calculated gauge-invariant quantities as functions of radius  $r$ , at a time slice midway between the turning points of the periodic solution, in units where  $M_W = 1$ . The Higgs boson mass is  $M_H = M_W$ . The left graph shows  $|\phi|^2$  (circles) and  $\text{Re}(\chi^*\phi^2)$  (squares); the right graph,  $|\chi|^2$  (circles) and  $r^2 f_{01}$  (squares). The curves are from the analytic expressions (3.2) for the instanton fields, with  $\rho \approx 0.0208/M_W$ ; the leading-order perturbative prediction is  $\rho \approx 0.0202/M_W$ .

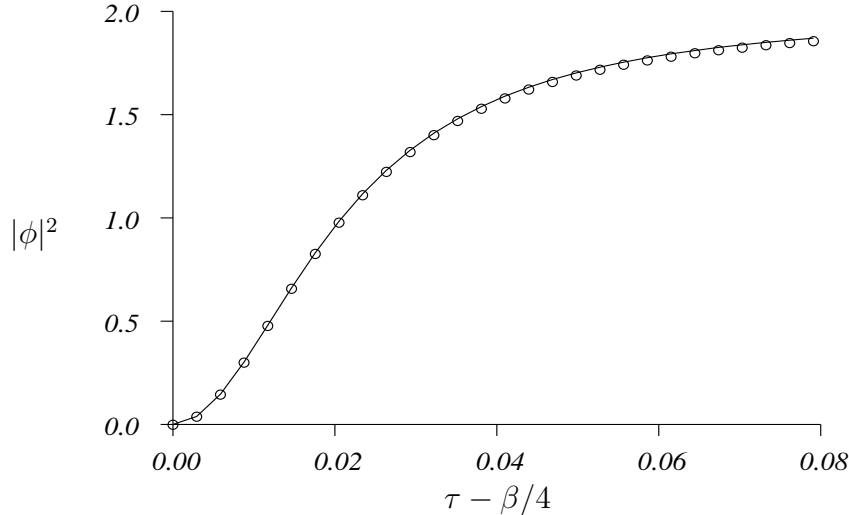


FIG. 7. The numerical bounce solutions approach instanton–anti-instanton fields, for small period ( $\beta = 0.75/M_W$ ). The circles show the field  $|\phi|^2$  as a function of imaginary time  $\tau$ , extrapolated to the spatial origin  $r = 0$ , in units where  $M_W = 1$ . The Higgs boson mass is  $M_H = M_W$ . The curve is from the analytic expression for the instanton field (3.2), with the same value of  $\rho$  as in Fig. 6.

## IV. DISCUSSION

At non-zero temperature, the leading exponential dependence of the semi-classical barrier crossing rate is set by the action of the periodic Euclidean solution (with period  $\beta$  equal to the inverse temperature) with least action. In electroweak theory, because of the anomaly in the baryon current, this barrier crossing (or topological transition) rate also gives the rate of baryon number non-conservation. For sufficiently low temperature, this rate is determined by the limiting action of zero-size instanton–anti-instanton configurations [1,6,5]. For higher temperatures, the rate is set by the action of the static sphaleron [3,4]. For Higgs boson mass  $M_H > 6.665 M_W$ , there is an intermediate range of temperatures just below the temperature  $1/\beta_0$  of the bifurcation point  $Q$ , for which the periodic Euclidean solutions we calculated numerically have a smaller action than the zero-size limit of instanton–anti-instanton configurations. In this range of temperatures, the action of these periodic Euclidean solutions determines the leading exponential behavior of the topological transition rate. As the temperature decreases, the action of the time-dependent periodic solutions eventually exceeds the action of zero-size instanton–anti-instantons. At temperatures below this crossing, the semi-classical transition rate is set by the zero-size instanton–anti-instanton action. For smaller Higgs boson mass  $M_H < 6.665 M_W$ , non-singular time-dependent periodic solutions never describe the dominant transition mechanism. Instead, the leading semi-classical transition rate undergoes an abrupt cross-over from sphaleron-dominated transitions to zero-size instanton–anti-instanton transitions, at the temperature where their actions cross.

Our numerical investigations were limited to real solutions of the Euclidean field equations. In addition to the real solutions we calculated, one may easily show that there are also complex branches of solutions which emerge from both bifurcation points  $P$  and  $Q$ . It is completely straightforward to extend the numerical techniques we employed to find these complex branches of solutions. This has been done by Bonini *et al.* [9]. On the branch emerging from the bifurcation  $Q$  at the sphaleron, there is a single “circle” of complex solutions related to one another by time translation symmetry.<sup>8</sup> Both parity and time translation by  $\beta/2$  act on this branch of solutions as complex conjugation; therefore the action of these complex solutions remains real, and decreases as one moves away from the sphaleron. These solutions are the analytic continuation to Euclidean space of real Minkowski-space solutions whose energy is greater than the sphaleron energy, and which are rolling toward, or away from, the sphaleron. Their precise initial conditions are determined by the requirement that they have a periodic analytic continuation to imaginary time.

For the other branch of complex solutions, emerging from the bifurcation  $P$ , there are

---

<sup>8</sup>To help understand the properties of these complex solutions, one may examine a simple algebraic model which reproduces the pattern of exact solutions, bifurcations, discrete symmetries, and negative and zero modes seen in the SU(2)-Higgs model. The toy model action is  $S[x, y, z] = S_0 - z^2/2 + \Omega r^2/2 + \lambda r^4/4 - r^6/6$ , where  $r^2 \equiv x^2 + y^2$ . Rotations in the  $x$ - $y$  plane correspond to Euclidean time translation. The origin,  $r = z = 0$ , represents the static sphaleron.  $z$  represents the amplitude of a deformation in the direction of the static negative mode of the sphaleron.  $x$  and  $y$  represent amplitudes of the  $\cos 2\pi t/\beta$  and  $\sin 2\pi t/\beta$  components of the fundamental sphaleron oscillation, respectively. Time reversal sends  $y \rightarrow -y$  leaving  $x$  and  $z$  unchanged. Parity combined with a  $\beta/2$  time translation sends  $z \rightarrow -z$  leaving  $x$  and  $y$  unchanged. Varying  $\Omega$  is analogous to varying the period  $\beta$  relative to  $\beta_0$ . Varying  $\lambda$  is analogous to varying the Higgs mass  $M_H$  relative to  $3.091 M_W$ . All the solutions we have discussed correspond to different extrema of  $S$  for either real or complex  $r^2$ .

two different “circles” of solutions (not related to one another by time translation) with complex action, and both parity and complex conjugation map one circle of solutions onto the other. The physical relevance of these particular complex solutions is not clear. However, complex solutions satisfying different boundary conditions are known to be relevant for non-perturbative scattering [8], and it would certainly be worthwhile to calculate those complex solutions explicitly.

### ACKNOWLEDGMENTS

The authors are grateful to S. Habib, E. Mottola, and R. Singleton for helpful discussions. This work was supported in part by the U.S. Department of Energy grant DE-FG03-96ER40956.

## REFERENCES

- [1] G. 't Hooft, Phys. Rev. D **14**, 3432 (1976).
- [2] F. R. Klinkhamer and N. S. Manton, Phys. Rev. D **30**, 2212 (1984).
- [3] V. A. Kuzmin, V. A. Rubakov, and M. E. Shaposhnikov, Phys. Lett. **155B**, 36 (1985).
- [4] P. Arnold and L. McLerran, Phys. Rev. D **37**, 1020 (1988).
- [5] S. Habib, E. Mottola, and P. Tinyakov, Phys. Rev. D **54**, 7774 (1996).
- [6] K. L. Frost and L. G. Yaffe, Phys. Rev. D **59**, 065013 (1999).
- [7] S. Coleman, Phys. Rev. D **15**, 2929 (1977).
- [8] S. Y. Khlebnikov, V. A. Rubakov, and P. G. Tinyakov, Nucl. Phys. **B367**, 334 (1991).
- [9] G. Bonini *et al.*, in Proc. of “Strong and Electroweak Matter ‘98,” Copenhagen, December 1998.
- [10] B. Ratra and L. G. Yaffe, Phys. Lett. B **205**, 57 (1988).
- [11] L. G. Yaffe, Phys. Rev. D **40**, 3463 (1989).
- [12] J. Kunz and Y. Brihaye, Phys. Lett. B **216**, 353 (1989).